Lab on a Chip

PAPER

View Article Online
View Journal | View Issue

Cite this: *Lab Chip*, 2015, **15**, 2808

Multiplexed paper analytical device for quantification of metals using distance-based detection†

David M. Cate,[a] Scott D. Noblitt,[b] John Volckens*[ac] and Charles S. Henry*[ab]

Received 26th March 2015,
Accepted 8th May 2015

DOI: 10.1039/c5lc00364d

www.rsc.org/loc

Exposure to metal-containing aerosols has been linked with adverse health outcomes for almost every organ in the human body. Commercially available techniques for quantifying particulate metals are time-intensive, laborious, and expensive; often sample analysis exceeds $100. We report a simple technique, based upon a distance-based detection motif, for quantifying metal concentrations of Ni, Cu, and Fe in airborne particulate matter using microfluidic paper-based analytical devices. Paper substrates are used to create sensors that are self-contained, self-timing, and require only a drop of sample for operation. Unlike other colorimetric approaches in paper microfluidics that rely on optical instrumentation for analysis, with distance-based detection, analyte is quantified visually based on the distance of a colorimetric reaction, similar to reading temperature on a thermometer. To demonstrate the effectiveness of this approach, Ni, Cu, and Fe were measured individually in single-channel devices; detection limits as low as 0.1, 0.1, and 0.05 μg were reported for Ni, Cu, and Fe. Multiplexed analysis of all three metals was achieved with detection limits of 1, 5, and 1 μg for Ni, Cu, and Fe. We also extended the dynamic range for multi-analyte detection by printing concentration gradients of colorimetric reagents using an off-the-shelf inkjet printer. Analyte selectivity was demonstrated for common interferences. To demonstrate utility of the method, Ni, Cu, and Fe were measured from samples of certified welding fume; levels measured with paper sensors matched known values determined gravimetrically.

Introduction

Human exposure to metal-containing particulate matter (PM) has been studied extensively. Epidemiological studies of metal exposure in the workplace have found that occupations such as metalworking, construction, transportation, and mining place individuals at increased risk to numerous cardiovascular and respiratory health issues, even to early death.[1] For example, inhalable aerosols containing Ni are listed by the International Agency for Research on Cancer as probably carcinogenic (Group 2B) to humans and animals.[2] Tens of thousands of individuals are exposed to metal-containing PM in their workplace, yet relatively few are routinely monitored for their exposure due to the time-intensive sampling and cost-prohibitive analytical methods currently available.[3] Common measurement methods for metals include inductively coupled plasma optical emission spectroscopy, mass spectrometry, and atomic absorption spectroscopy.[4,5] These analytic methods have high precision, sensitivity, and low detection limits, but they are expensive (>$100 per sample) and require trained specialists for operation.

Low-cost, point-of-need sensors have been highlighted as key for improving exposure assessment.[6] Towards this goal, microfluidic paper-based analytical devices, or μPADs, have shown promise for overcoming technical and financial obstacles that, traditionally, have impeded more widespread exposure assessment. One major limitation of current exposure analysis methodologies is cost; therefore, detection strategies need to be minimally instrumented yet sensitive enough for routine monitoring. Paper sensors are attractive as an analytical tool because sample flow is passively driven by capillary action, microliter sample and reagent volumes are needed, and devices (typically) are disposable. To date, paper sensors have been developed for environmental exposure analysis of various agents, including: metals,[7–11] pesticides,[12] explosive residues,[13,14] and reactive oxygen species,[15,16] among others. However, μPADs still have limitations; they often require external equipment, trained personnel, and are not geared for multiplexed analyses.

To date, the most common detection motif for paper sensors has been colorimetry.[17,18] Although straightforward, accurate quantification of color intensity on paper requires

[a] *School of Biomedical Engineering, Colorado State University, Fort Collins, Colorado 80523, USA. E-mail: John.Volckens@colostate.edu, Chuck.Henry@colostate.edu*
[b] *Department of Chemistry, Colorado State University, Fort Collins, Colorado 80523, USA*
[c] *Department of Mechanical Engineering, Colorado State University, Fort Collins, Colorado 80523, USA*

† Electronic supplementary information (ESI) available. See DOI: 10.1039/c5lc00364d

an external optical detector (*e.g.* camera, scanner, *etc.*) and image quality has been known to vary based on lighting conditions.[19] Alternatively, visual detection using a color/intensity comparator can be used; however, color hue and brightness perception may differ from person to person, complicating analysis and increasing measurement uncertainty. Several groups have made attempts to simplify quantitative readout by removing all external instrumentation. One strategy employed by Lou *et al.*[20] involved counting the number of segments (along a flow path) that reacted with analyte, where the number of segments was proportional to analyte concentration. This detection motif has since been applied for measuring hydrogen peroxide.[21,22] Using time as an analytical readout has also been explored.[23] A timing element (*e.g.* stopwatch, phone app) measured the time elapsed for a chemical reaction that took place between an analyte and indicator. A complementary approach originally developed by Zuk *et al.* in 1985,[24] and later expanded by our group, is distance-based detection.[25] This technique relies on reading the length of a colored reaction product along a paper channel with the unaided eye. Each device essentially contains one sample reservoir and a flow channel patterned with a colorimetric indicator specific for an analyte of interest. As analyte flows down the channel, complexes formed between analyte and indicator precipitate, generating a color band with a length that is proportional to the amount of analyte present. Visual quantification is aided by a ruler printed alongside each device, similar to reading temperature on a thermometer. In this approach, analyte is measured completely with the unaided eye; no electronic readers or timers are necessary.

A key step in consistent color formation on paper is reagent deposition. In porous networks, color formation is dependent on wicking rate, which decreases nonlinearly with time/penetration distance in paper.[26–28] In distance-based detection, analytical dynamic range is heavily influenced by wicking behavior. Slower flow rates allow more time for reaction in a given zone, ultimately leading to a shorter band of color along the detection channel and a smaller dynamic range. To address this limitation, concentration gradients of a chromophoric indicator were printed along the channel using a modified piezoelectric printer.[29,30] Inkjet printing has become a common fabrication technique for defining the location and concentration of chemical reagents on paper surfaces.[31] Many of the reported printing techniques for μPADs use hydrophobic barriers for confining reagents,[32–35] though it is becoming more common to pattern reagents directly on the substrate surface.[36–38] Reagent printing is advantageous because it greatly improves device reproducibility, functionality, and flexibility compared to manual deposition methods such as pipetting, nebulizing, or dip coating. Small droplet volumes from the printer (~1.5 pL) lead to high patterning resolution and little reagent is wasted in the manufacturing process. Moreover, inkjet printing is scalable for mass production.

In this work, a distance-based μPAD was developed for simultaneous measurement of Fe(II), Ni(II), and Cu(II) from aerosolized particulate matter. These metals were selected due to their high prevalence in welding fumes. Typically, metals are extracted from filter samples for chemical speciation, but in this work we utilized certified welding fumes in powder form. Hydrophobic barriers and colorimetric reagents were printed for controlling fluid transport and for quantifying metals. Reagent deposition by inkjet printing provided better assay reproducibility than manual deposition (6.3% *vs.* 11.4% relative standard deviation). The limit of detection for Ni, Cu, and Fe in single and multi-channel devices was 0.1, 0.1, 0.05 μg (6.7, 6.7, 3.3 ppm) and 5, 5, 1 μg (100, 100, 20 ppm), respectively. Chemical gradients were printed to extend the dynamic range of each assay; improvements of 50.0% and 41.2% were observed for Ni and Cu. Signal interference from non-target metals was also investigated. Metal constituents common to most welding alloys (*e.g.* stainless and mild steel) had minimal impact on results. Finally, a welding fume standard certified for Mn, Fe, Ni, and Zn was used to demonstrate the efficacy of distance-based detection for measuring metal particulates in samples with complex matrices.

Experimental methods

Materials and equipment

All reagents were analytical grade. Ultrapure water (18.2 MΩ cm) from a Mill-Q system (Merck Millipore, Darmstadt, Germany) was used throughout. Laboratory containers were rinsed with H_2O prior to use. Standard solutions of all metals (lead(II) nitrate, cadmium(II) nitrate tetrahydrate, potassium dichromate(VI), iron(III) chloride hexahydrate, nickel(II) sulfate hexahydrate, copper(II) sulfate pentahydrate, manganese(II) chloride tetrahydrate, magnesium(II) chloride hexahydrate, iron(II) sulfate heptahydrate, aluminum(III) sulfate hydrate, barium(II) chloride, vanadium(III) chloride, and cobalt(II) sulfate pentahydrate) were purchased from Sigma-Aldrich (St. Louis, MO, USA). L-ascorbic acid (97%), L-cysteine, tris base (99.9%), bathophenanthroline (97%), dimethylglyoxime (99%), dithiooxamide (98.5%), and sodium fluoride were purchased from Sigma-Aldrich. Sodium acetate, ammonium acetate, hydrochloric acid, sodium hydroxide, and glacial acetic acid were obtained from Fisher Scientific (Pittsburgh, PA, USA). Whatman (grade 1) filter paper was purchased from Apollo Presentation Products (Booneville, MS, USA).

Device fabrication and operation

Distance-based detection with μPADs has been described previously.[25] The operational concept for multiplexed distance-based detection is shown in Fig. 1. Briefly, a wax barrier designed in a shape resembling a thermometer was printed onto Whatman 1 filter paper. To preserve channel resolution, wax barriers were printed on both sides of the filter paper. Each flow lane of the device served as a detection channel for a single metal. Analyte was added to the device at a circular reservoir at the bottom of the device, which formed a common flow inlet for all three channels. Filter paper containing

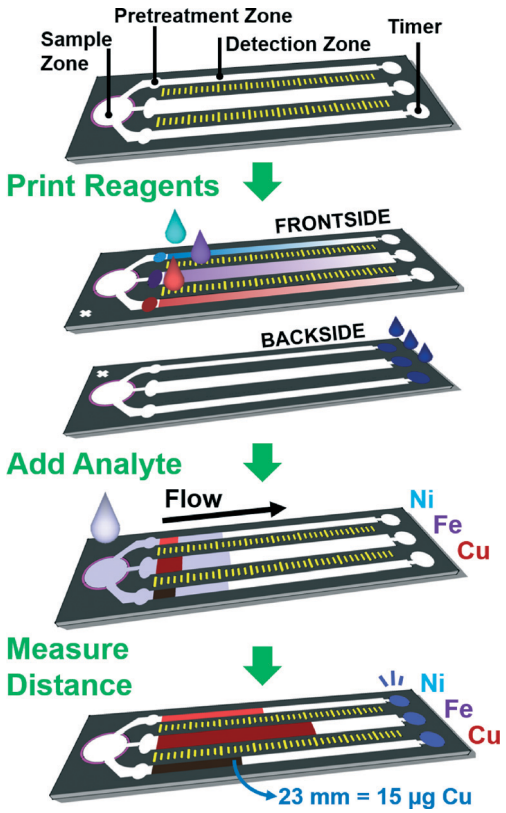

Fig. 1 Schematic of distance-based detection in a multi-layer device. Colorimetric reagents, buffers, and masking agents are inkjet printed in the detection and pretreatment zones. A colorimetric indicator was printed on the back of the device, functioning as a passive timer. Analyte mass was quantified when a metal-ligand complex precipitated on the substrate, generating a band of color with a length proportional to the amount of metal present. Quantification in single and multi-channel devices was achieved in ~30 and ~40 min, respectively.

either pretreatment reagents or the analyte may also be added to the reservoir to facilitate sample transfer into the detection zone. In this work, a piezoelectric printer (Epson R280) was used to deposit colorimetric detection reagents along the flow channel homogeneously or as a gradient. The primary component of the printed ink solution was isopropanol, so evaporation after printing was nearly instantaneous at the small volumes printed. Before adding sample, the devices were laminated (Apache AL13P) at 170 °C to create an encapsulating hydrophobic barrier to prevent solvent evaporation along the channel during analysis. A sample reservoir was punched using an 8-mm biopsy punch (Robbins Instruments, Chatham, NJ, USA) and backed with transparent tape to prevent leakage of solvent. As aqueous sample (50 μL) was added to the device *via* the sample reservoir, capillary action carried solution along the flow channel (the 3D wax barrier served to confine and direct sample flow). As analyte reacted with the colorimetric reagent deposited along the flow channel, a colored precipitate formed. Color development ceased once all the analyte had been consumed, though the eluent continued to proceed along the flow channel. Analyte quantification was achieved by measuring the distance of color development along the flow channel using a ruler printed beside each channel. A desktop scanner and computer software (Xerox DocuMate 3220 Scanner, color photo setting, 600 dpi) were also used to quantify color distance for experimental validation.

After sample addition, the eluent flowed along each channel until reaching a circular indicator zone at the end of the channel. Each indicator zone was pre-patterned with blue dye on the bottom of the device. When dry, the dye was not visible from the top of the sensor. Once wetted, dye in the indicator zone migrated from the bottom of the device to the top, indicating assay completion. The time from sample addition to appearance of the indicator dye was 40 ± 6 min (n = 10).

As described previously, the Reynolds number along the sample channel was low (~10), indicating laminar flow.[25] Color distance was measured from the beginning of the ruler printed beside each channel to the most downstream tip of detectable color (*i.e.*, the apex of the colored flow profile). The tip of color was chosen for detection rather than the furthest region spanning the width of the channel because both methods provided approximately the same level of reproducibility (6.1 and 6.5% RSD respectively), and the difference in analyte concentration in choosing one method over the other was lower than the limit of quantification for each assay.[25]

Inkjet cartridge modification and reagent printing

A piezoelectric inkjet printer (Epson Model R280) was selected for reagent printing, as described earlier, with modifications.[29,39] The purpose of inkjet printing was twofold: 1) printing offered superior control (*vs.* manual deposition) over the volume and droplet resolution of deposited material, and 2) this method enabled printing of non-uniform reagent concentrations onto the paper substrate. To modify the printer, stock Epson ink cartridges were replaced with third-party refillable cartridges (Inkproducts.com) which had been modified to fit 200 μL (non-filtered) pipette tips. For the cartridges, a Dremel® tool was first used to cut off the plastic nozzle protruding from the cartridge. A hole was then drilled from the bottom of the cartridge towards the top with drill bits of increasing size (1/4″ and 19/64″); care was taken not to extend the bit beyond the top of the cartridge. The sides of the cartridge remained intact. Compressed air was used to remove plastic remnants from inside the cartridge. Pipette tips used as ink reservoirs were cut to fit on nozzles over the print head (Fig. S1†). The tips were designed to fit tightly over the nozzles (*i.e.* without leaking). Inkjet reservoirs were cleaned with filtered H_2O, methanol, ethanol, and isopropanol, according to previous reports.[39] Approximately 100 μL of reagent solution (the composition varied according to each metal species) was injected into the pipette reservoir and pushed through the print head *via* a pipette until solution was dispensed onto a paper towel placed below the print head. After this 'priming step', another 180 μL of reagent solution was added to the reservoir. Adobe Illustrator CS3 software was used for device design and printing control. For

reagent printing, the highest available print quality was selected, and high-speed printing, edge-smoothing, and grayscale printing were deselected. Adobe RGB 2.2 was used for color control.

For each metal, concentration gradients were printed according to an empirically derived equation that determined the concentration of reagents deposited along the channel. Reagent concentration (*i.e.*, the number of successive overprints across a substrate) varied for each metal; for gradients, the concentration of reagent deposited was highest near the sample zone and decreased along the channel's longitudinal axis. A consequence of gradient printing was that the response curve for each metal was more linear, according to a residual sum of squares regression. As reagent concentration increased, the slope of the response curve (*i.e.* sensitivity) decreased (Fig. S5†). For each metal, the concentration of printed reagents were chosen to provide the highest linear dynamic range according to Tukey's range test and a test of non-linearity at 95% confidence. After reagents were added, each print head reservoir was flushed with ≥10 mL of H_2O, methanol, ethanol, and isopropanol to ensure complete removal of residual reagent.

Ink formulation and gradient creation

A solution composed of 95/5% (w/v) isopropyl alcohol/H_2O was used for all experiments as the solvent for colorimetric reagents, buffers, masking agents, and the indicator dye. Solution formulation was based on the reciprocal of the Ohnesorge number $Z = \mathrm{Oh}^{-1}$:

$$\mathrm{Oh} = \frac{(d\rho\gamma)^{1/2}}{\eta},$$

which is a function of the print head diameter d, and the fluid properties of surface tension γ, density ρ, and dynamic viscosity η. Much of the literature agrees that a Z value from 1–10 is ideal for producing consistent drops with minimal satellite spray, though debate persists about how large Z can be while maintaining high-quality droplet formation.[40] In this work, several organic solvents (isopropanol, ethanol, methanol, dimethylsulfoxide, xylene) were evaluated as candidates for printing; their Z values are listed in Table S1.† The Z value of isopropanol (16.4) was closest to ideal and was selected for printing. H_2O (5% w/v) was added to the isopropanol ink to increase solution surface tension.

Fluid velocity in porous networks is nonlinear, and because distance-based detection is velocity-dependent, the response (*i.e.*, color distance) generated for a range of metal masses is also non-linear. To counter this non-linearity in response, we developed equations for printing concentration gradients of colorimetric reagents on paper. The general process for creating a printed reagent gradient for detection of each metal was as follows: 1) measure the location of the eluent flow front, x_i, as a function time, t, along the longitudinal flow axis, 2) create a curve fit of x_i *vs.* t, 3) non-dimensionalize flow distance *vs.* time by creating parameters $x_i^* = \frac{x_i}{x_f}$ and $t^* = \frac{t}{t_f}$, where the variables x_f and t_f represent the maximum recorded distance x_f, of the fluid front at time t_f, 4) develop a new function representing the change in pixel intensity *vs.* distance (in pixels) along the channel [$I(D) = 255 \times x^*$] where $D = 215 \times t^*$ represents the distance of the fluid front in pixels. The coefficients 255 and 215 represent the maximum pixel intensity (in RGB space) and channel distance (in our system), respectively, 5) generate a counter function, $G = 255 - I(D)$, to be the complement of $I(D)$, 6) convert the counter function into a colored image using a custom-designed LabVIEW VI, and 7) print the gradient on the substrate at the desired concentration determined by the counter function (Fig. S2†). For gradient deposition, intensity equations used to create the gradients are provided in the supporting information. Colorimetric reagent concentration was optimized for each metal to produce the greatest linear dynamic range and lowest limit of detection. Statistical treatment of the data excluded outliers; a weighted linear regression was applied to each response curve due to unequal variance present in the sample measurement (Excel and LabVIEW software).

Nickel detection

Detection chemistry for Ni was used as previously reported, with modifications.[25] A solution composed of dimethylglyoxime (100 mM) and tris base (50 mM, pH 10.2) was made in 95/5% isopropanol/H_2O solvent. Masking agents (1 M NaF and 6 M ammonium acetate) were mixed 2 : 1 (%w/v) and applied to the pretreatment zone of the Ni detection channel five times *via* pipette (0.35 μL increments). The presence of sodium and ammonium acetate helped create a more visible color band in the channel and also served to mask potential interferences from Co and Fe.[7] The DMG solution was printed six times on each device (~3 μmol DMG per 20 devices) for both gradient and non-gradient reagent deposition. Sample volumes of 15 and 50 μL were deposited in the sample zone for analysis of Ni using the single-channel and multi-channel devices, respectively. For analysis, 1000 or 2000 ppm solutions of Ni(II), Cu(II), or Fe(II) were made and diluted with H_2O to appropriate concentrations. The Ni(DMG)H_2 complex is reddish pink and precipitates upon formation.

Copper detection

Measurement of Cu was carried out using dithiooxamide, a common ligand used for complexing Co, Ni, and Cu.[41] For detection, a solution composed of dithiooxamide (30 mM), sodium acetate buffer (pH 4.0, 20 mM), and 1% (w/w) hydroxylamine was made in 95/5% (w/v) IPA/H_2O solvent. For masking, a solution of higher hydroxylamine concentration (10% w/w in H_2O) was made and added *via* pipette to the pretreatment zone of the Cu detection channel once (0.35 μL). At low pH, the binding constant for Ni to dithiooxamide was reduced, preventing much of the Ni from

interfering with Cu measurement. Quantitative recovery of Ni with dithiooxamide has been typically performed from pH 7–9.[42] Chemical gradients for detection of Cu were printed seven times (~1 μmol dithiooxamide per 20 devices).

Iron detection

Measurement of Fe was carried out using 4,7-diphenyl-1-1,10-phenanthroline (bathophenanthroline), a common colorimetric indicator for Fe corrosion.[43,44] Bathophenanthroline (Bphen) was selected as the chromogenic reagent for Fe over other common 1,10-phenanthroline derivatives because 1) Bphen is approximately two times more sensitive to Fe than 1,10-phenanthroline, 2) the ferrous-Bphen complex has low solubility in H_2O, and 3) Bphen has fewer interferences than 1,10-phenanthroline for Fe detection. A solution composed of Bphen (10 mM), sodium acetate buffer (pH 4.5, 20 mM), and 1% (w/w) L-ascorbic acid was made in 95/5% (w/v) IPA/H_2O solvent and printed twenty times along the Fe detection channel (~1 μmol Bphen per 20 devices). Ascorbic acid (5% w/w) was added to the pretreatment zone *via* pipette (0.5 μL) to reduce soluble Fe(III) to Fe(II) for complexation with Bphen.

Welding fume standard reference material

A reference material derived from stainless steel welding fume (HSL SSWF), certified for Fe, Mn, Ni, and Zn was obtained from the Health and Safety Laboratory (Harpur Hill, Buxton, UK). Approximately 1 mg of the HSL SSWF was weighed and added to a 1.5 mL centrifugation tube, followed by acid digestion under 10 μL HCl (15.4 M) and 15 μL H_2O. Each aliquot was then microwaved (1100 W) for 6 min, before adding 25 μL NaOH (3 M). Aliquots were centrifuged for 3 min at 10 000 RPM. Extracted supernatant (volume varied) was diluted with H_2O to a total volume of 50 μL prior to use. Control tests were conducted in parallel using standard metal solutions.

Data analysis

Measurements were recorded with half-millimeter resolution using rulers printed beside each detection channel; distances measured visually were later verified with Image J software using images obtained from a scanner. Outliers were discarded when identified using Grubb's test for outliers.[45] Assumptions of normality and unequal variance were verified using chi-squared and F distribution tests. Minimum sample sizes for testing were determined using a power analysis ($1 - \beta \geq 0.8$, $\alpha = 0.05$, using G*Power v3.1.9.2 software). Due to the presence of increasing variance with metal mass, we applied a weighting factor to each linear regressed fit of the data (Fig. S3†). In this work, weighting (w) was given according to inverse distance (y_i^{-1}), according to the equation:

$$w_i = \frac{n y_i^{-1}}{\sum_{i=1}^{n} y_i^{-1}}$$

where n is the number of samples in the calibration data set.

3. Results and discussion

3.1 Detection of Fe, Ni, and Cu in single channels

For each metal, single-channel devices were fabricated and patterned with reagents to determine detection sensitivity, detection limits, and operating range. Quantitative values are provided in units of mass because the target sample comes from air pollution; equivalent concentration units are provided in parenthesis throughout the paper. Initial studies were performed by nebulizing colorimetric reagents on the paper substrate, as described previously,[25] to ensure uniform coverage along the detection channel. Standard metal solutions from 0.01–100 μg (0.7–7 × 10^3 ppm) were made for each metal; for each test 15 μL was added to the sample zone of the device. The dynamic ranges for Ni, Cu, and Fe were 0.1–5, 0.1–10, and 0.05–7 μg, respectively ($n \geq 10$). The upper limit of the range for each metal was determined by applying the Tukey–Kramer range test. Limit of detection was determined by the lowest measurable distance of the color band that precipitated a minimum of 1 mm from the beginning of the detection channel (as identified by a 0 mm datum printed onto device). Relative standard deviations ranged from 9.5–13%, which is typical with μPADs.[13] A higher molar extinction coefficient for the complex was hypothesized as the reason for a 50% improvement in detection limit for Fe(II)-Bphen (2.2 × 10^4 M cm^{-1}) compared to Ni(DMG)H_2 (3 × 10^3 M cm^{-1}) and Cu-dithiooxamide (750 M cm^{-1}).[46–48] The observed solubility of the Ni(DMG)H_2 complex was higher than the Cu-dithiooxamide product, which was suspected as the reason why detection sensitivity of Ni was not higher than Cu.

3.2 Extending dynamic range

A constant reduction in wicking rate was a factor limiting the upper range of detection; over time, the rate of flow approached zero, ceasing new color formation along the detection channel. To overcome this limitation, two approaches were tested: 1) control channel geometry, and 2) control colorimetric reagent concentration.

3.2.1 Varying channel width. The hydrophilic surface available for reagent-analyte complexation influenced the slope of the analyte response curve. More paper surface (per unit distance along the flow channel) led to a lower sensitivity (less positive slope) than when less paper surface was available (more positive slope). However, because the flow in the paper channel followed Lucas–Washburn theory,[49] sample flow rate eventually approached zero (in our system this occurred ~60 mm down the channel). As the sample flow rate approached zero, further growth of the color band ceased. As a result, a tradeoff exists between dynamic range and sensitivity for distance-based detection with μPADs. This tradeoff, lower dynamic range for higher sensitivity and *vice versa*, is depicted using two hypothetical traces in Fig. S4.† In the figure, the linear dynamic range of trace 1 (1–34 μg) is approximately 48% smaller than the linear dynamic range of trace 2 (1–70 μg). To minimize upper-bound losses, a study was performed with single-channel devices with widths

starting at 4.7 mm and decreasing in 25% increments (*e.g.* 4.7, 3.5, and 2.6 mm). Channel width was defined prior to melting the wax barrier (Fig. 2). According to previous work, 2.6 mm was subjectively chosen as the narrowest channel width for which a visual reading of the color band could be accomplished without difficulty by the naked eye.[25] The maximum channel width was limited to 4.7 mm because detection range for wider channels was unacceptably low. As demonstrated in Fig. 2, the slope of the response curve for Fe decreased in devices from the narrowest to widest channel, as anticipated. The detection limit was not influenced by channel width in this study and was equal for all three experiments. We suspect this was due to a threshold of analyte mass that must be present before color formation was visible with the unaided eye. A channel width of 3.5 mm was chosen for this study because it produced a response curve with the best sensitivity and largest dynamic range for Fe. Although the dynamic range of channels 4.7 mm wide was slightly larger (Fig. 2B), the slope of the response curve was low, prompting our decision to pursue testing with 3.5 mm channels. Further alterations of channel geometry were not considered for this study but could potentially provide a larger overall dynamic range for metals. Narrow channels produce higher sensitivity (good for low analyte levels), but were non-ideal for larger analyte concentrations because less surface available for analyte-reagent complexation produced a longer band of color. Due to a constant reduction in eluent flow rate with penetration distance in the channel, long (*i.e.* >50 mm) color bands were undesirable because eluent velocity beyond 50 mm was approximately zero.

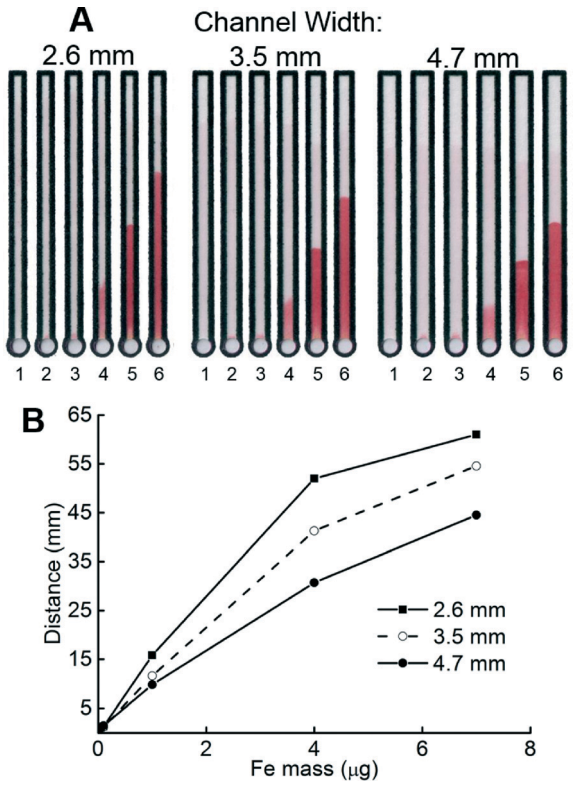

Fig. 2 (A) Detection sensitivity for Fe(II) varied as a function of channel width. (B) Quantitative data from (A). As channel width increased, the sensitivity (slope) of Fe(II) measurement decreased.

3.3 Distance-based detection of Ni, Cu, and Fe in single channels

Gradients of colorimetric reagents were printed 1–25 times in odd-numbered increments (Fig. S6†); devices were tested with the same analyte range (0.1–20 μg) for all three metals. If two or more concentrations produced the same linear dynamic range, preference was given to the concentration that produced the highest sensitivity (slope). The dynamic ranges for Ni, Cu, and Fe were 0.1–10, 0.1–17, and 0.05–7 μg, respectively ($n \geq 10$). Relative standard deviations ranged from 6.0–6.6% (Fig. 3). From an exposure perspective, these linear ranges correspond to metal aerosol concentrations (as time-weighted averages) from 1.43–143, 1.43–242, and 0.710–99.8 μg m^{-3} assuming analysis is performed using a 10-mm filter punch extracted from a 37-mm filter operating at 2 L min^{-1} of air flow.[50] Time-weighted averages are used in occupational air sampling to calculate a welder's exposure to a hazardous substance, averaged over an 8 hr shift.[51] When compared to the minimum action level for a substance, the time-weighted average exposure determines if a person has been exposed to a toxic concentration of a metal species (action levels vary by metal). If the average exposure is above the action level, corrective action such as more frequent exposure monitoring and medical surveillance must be taken to mitigate undue risk.[50] A comparison between the analyte ranges that were measurable between gradient printing and manual reagent deposition (spraying) showed that printing extended the dynamic range by 50, 41, and 0% for Ni, Cu, and Fe, respectively. Results are displayed for all three metals in Fig. 3. The difference in Fe performance compared to Ni and Cu is unclear and is under investigation. However, the linearity of the Fe assay was still improved. By extending the dynamic ranges for Ni and Cu, a greater range of exposures can be analyzed. The TWA's for Ni, Cu, and Fe are all below the permissible exposure limits (1000, 100, and 1000 μg m^{-3}, respectively) established by the Occupational Safety and Health Administration.[50] This means that shorter sampling times can be used to capture task-based exposures instead of relying on an ensemble average over the course of a full day. Reagent printing also exhibited a significant improvement in relative standard deviation (from 11.4 to 6.4% on average) compared to manual deposition. Visual differences for the detection of Cu (1–13 μg) between devices in the presence and absence of a colorimetric reagent gradient are demonstrated in Fig. 4. For a given Cu mass, the measured color band was longer in the presence of a gradient. This difference was magnified at higher Cu masses. The average differences between band distance for devices with and without gradients for Cu masses of 1, 4, 8, and 13 μg were 3.6, 7.9, 10.7, and 15.2 mm, respectively.

For single-channel μPADs, the limit of detection was much higher for Ni, Fe, and Cu (7, 3, and 7 ppm), respectively, than

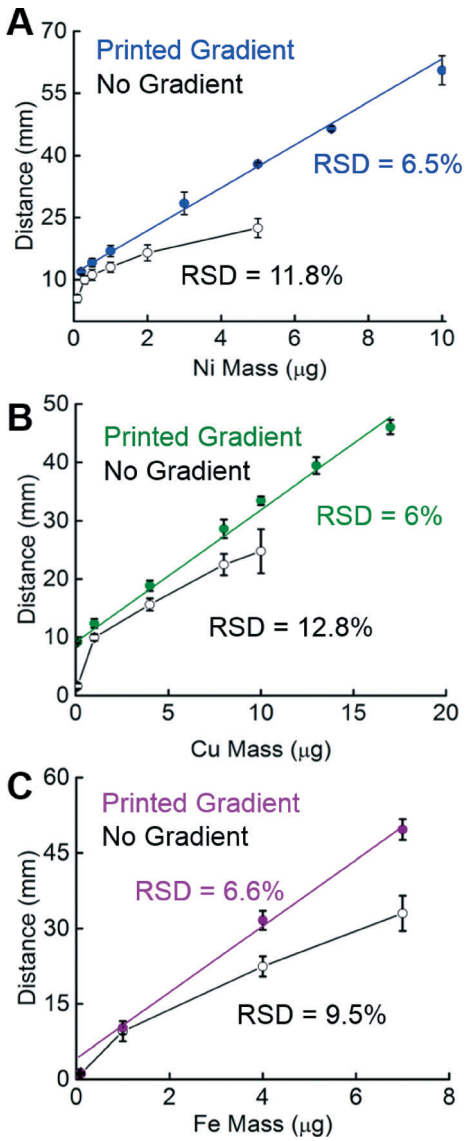

Fig. 3 Distance-based detection of (A) Ni, (B) Cu, and (C) Fe. Printing a concentration gradient increased the linear dynamic range of Ni and Cu by 50 and 41%, respectively, than in the absence of a gradient. Inkjet printing was also more reproducible than manual reagent deposition ($n \geq 4$).

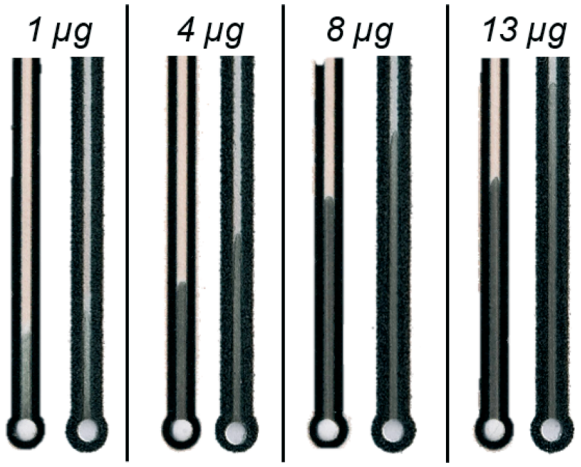

Fig. 4 In the presence of a reagent gradient, the distance of the color band increased as a function of the mass of Cu added. For each set of devices, the left and right images were in the absence or presence of a reagent gradient. In the absence of a gradient, reagents were deposited evenly across the substrate surface.

for inductively-coupled plasma – optical emission spectroscopy (1–10 ppb). Perhaps the most common detection technique for heavy and transition metal detection, ICP-OES is certainly sensitive, however the cost of analysis (on a per-sample basis) is several orders of magnitude higher than for the μPAD technique presented here. Another common analytical method, X-ray fluorescence spectroscopy, is less expensive than ICP, but detection limits are not appreciably better than with μPADs (sub 10 ppm).

3.4 Simultaneous distance-based detection of Ni, Cu, and Fe

3.4.1 Multi-channel device geometry. Device inlet geometry was investigated for the multi-channel format. At neutral pH, the overall charge at the surface of cellulose was negative, which could hinder cation transport in the device through electrostatic interaction. We hypothesized that a device with more inlet surface area would lead to higher metal detection limits because, when present at low mass, metal analyte was sufficiently hindered by the cellulose matrix (and thus, some proportion of each sample failed to reach the detection zone). Two devices with varying inlet surface areas, A and B, were tested; reagent concentrations, solution pH, masking agents, and detection channel geometry were equivalent between both devices (Fig. S7†). Device A had approximately 66% more inlet surface area than device B. The mass of Ni tested for both devices ranged from 5–80 μg. The limits of detection for devices A and B were 20 and 5 μg, respectively. Both devices responded similarly (*i.e.* not statistically differently) above 35 μg Ni.

A droplet of solution added to the sample zone wicked towards the detection channels as a result of capillary action. The path length from the sample zone to either Ni or Cu channels was longer than for Fe. The result was that fluid fronts for Ni and Cu significantly lagged (*i.e.* minutes) behind the front for Fe. Two approaches were sought to produce equivalent volumetric flow rates in all channels: 1) increase the length of the flow path to the Fe channel, and 2) decrease the width of the flow path to the Fe channel, creating a constriction that limited the flow rate of eluent to the Fe channel. An elongated flow path extended the time for the fluid front to travel from the sample to detection zone; however, we observed significant analyte losses to the capillary network as a result of chemical interactions between cationic metals and cellulose (data not shown). We opted for the second method, testing a variety of lengths and widths of constriction channels bounded by wax barriers, before settling on a channel 500 × 750 μm ($W \times L$) after melting with a laminator. Channels narrower than 500 μm were not reproducible.

3.4.2 Analyte measurements. Three single-channel devices were combined in parallel for simultaneous measurement of Ni, Cu, and Fe. ESI† movies M1 and M2 demonstrate measurement of metals in two- and three-channel formats. Design changes implemented in the multi-channel device were: dual rulers printed between detection channels for easier analyte quantitation, a larger sample well to accommodate higher-volume droplets and larger samples (3 *vs.* 8 mm), wide wax barriers (4.2 mm before melting) between channels to mitigate cross-contamination, and a passive timer. The passive timer was composed of a blue dye (food coloring) printed at the end of each detection channel on the underside of the device which was allowed to dry. When eluent reaches the end of the detection channel, the dye was solubilized and quickly migrated to the top of the device. Thus, the presence of blue dye indicates the assay completion. A time lapse of detection is presented in Fig. 5a for 5, 5, and 15 μg Ni, Cu, and Fe, respectively. This automated indicator system is simple, removes all external timing mechanisms, and reduces potential error due to assay timing. Moreover, timing for each channel is independent of the others; complications in any one channel will not impede analyte measurement in the other two.

Eluent flow rates were measured in the multi-channel system to establish empirical equations for reagent gradient printing. Future efforts will be directed towards establishing predictive flow models in these devices, eliminating the need for empirical fits. Linear dynamic range, detection limits, and device reproducibility were investigated using serially diluted analytical standards (2000 ppm). Metal ranges varied from 1 to 100 μg. The linear dynamic ranges presented in Fig. 5b for Ni, Cu, and Fe were 5–55, 1–65, and 5–65 μg, respectively ($20 \leq n \leq 32$ per mass). Relative standard deviations ranged from 6.7–8.4% (7.6% average). For aerosol exposure monitoring, time-weighted averages for these range values are 71.3–784, 14.3–927, and 71.3–927 μg m^{-3}, respectively. The relative standard deviation was slightly higher (7.6%, up from 6.4%) for the multi-channel device than for assays conducted in single channels likely due to greater variance present in device fabrication (*e.g.* variation in width of constriction channel). A comparison between single- and multi-channel devices is presented in Table 1. The mass of analyte that was measurable was likely higher for the multi-channel device due to analyte losses from flow in paper and from analyte splitting as a result of operating parallel channels. In the multi-channel format, analyte was split between three channels. Ni and Cu channels each occupy ~25% of the available surface area for detection meaning that the mass of analyte entering either channel was decreased (*vs.* a single-channel device) by ~75%.

To quantify intra- and inter-device variability, assays were conducted for all three metals with large sample sizes (*i.e.* $n > 100$). A minimum of three independent reagent solutions were made, and at least three separate sheets of devices were fabricated per metal. Reagent printing was performed over the course of one week. Weighted confidence and prediction intervals ($\alpha = 0.05$) are provided in Fig. S3† for Ni, Cu, and Fe. Capturing the variability present in solution preparation, reagent printing, and device fabrication enabled us to quantify the error around the measurement of a single unknown sample, which is relevant for actual use in the field. When measuring Ni, for example, if the nominal mass being measured were 15 μg (lower end of dynamic range), we would expect the multi-channel device to measure distances ranging from 9–13 mm, corresponding to a measured Ni mass between 12–18 μg, which is ±20% ($n = 140$). If the nominal mass measured were 45 μg (higher end of the dynamic

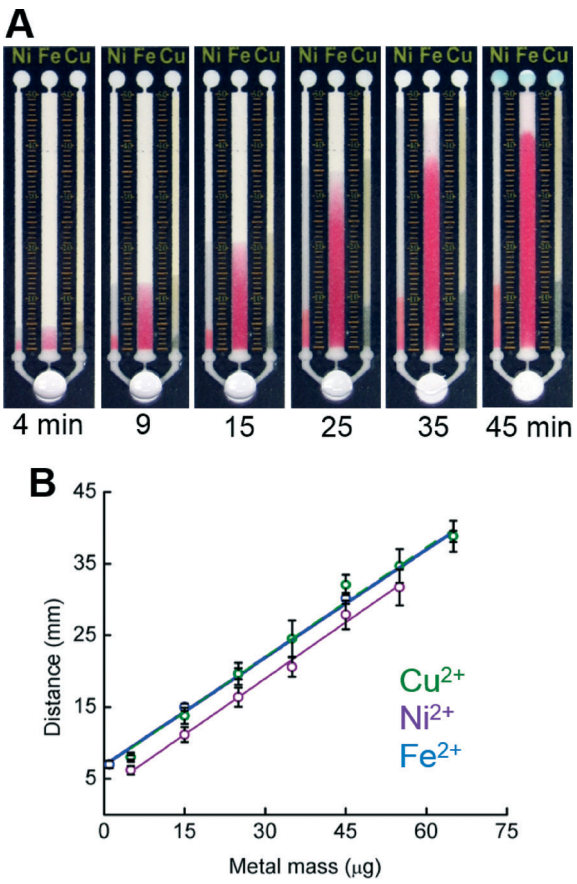

Fig. 5 (A) Time lapse of 15, 5, and 5 μg Fe, Ni, and Cu. (B) Response curves for Cu, Ni, and Fe in the multi-channel device.

Table 1 Comparison of dynamic range and percent relative standard deviation for single and multi-channel devices for analyte mass (concentration). $n \geq 100$

Metal	Single channel (μg) (ppm)	Multi-channel (μg) (ppm)	Single-channel (Multi-channel) %RSD ($n \geq 10$)
Ni	0.10–10 (6.7–670)	5.0–55 (100–1100)	6.5% (6.7%)
Fe	0.05–7.0 (3.3–470)	1.0–65 (20–1300)	6.6% (7.7%)
Cu	0.10–17 (6.7–1100)	5.0–65 (100–1300)	6.0% (8.4%)

range), we would expect distances between 23–30.5 mm (37–53 μg Ni, which is ±18%).

3.5 Interferences

Welding fumes contain numerous metal and gaseous compounds. Respirable fume composition varies based on the welding technique performed and on the composition of the welding rod, flux, shielding gas, and metal substrate being welded.[52] Stainless steel, perhaps the most common commercially welded metal, contains large quantities of Ni (6–15% wt%), Cr (16–24% wt%), and Fe (≥50% wt%). A short list of common metal alloys and their chemical composition is provided in Table S2.† The complexity of the welding-fume matrix suggests that other metal species may interfere with our analysis, so a tolerance study was performed. The tolerance ratio is defined as the mass of metals that generates less than a 10% change in the distance measured *versus* the control, for Fe, Ni, and Cu.[53] Analytes, Fe, Ni, and Cu, were held at 10 μg while the mass of each interfering metal species varied according to the ratio (μg interference per μg analyte) presented in Table 2. Interfering metals were not evaluated above 10× the analyte mass. From the results, it was determined that Ni(II), Fe(II), Zn(II), Co(III), Cd(II), Pb(II), Mn(II), V(III), Mg(II), Al(III), or Ba(II) did not interfere with distance-based detection of Fe, Ni, or Cu based on the average chemical composition of stainless or mild steel. The relative percent composition of Ni in most metal alloys is not expected to reach 0.5× of Fe. Similarly for Co(II), the percent composition should rarely meet or exceed that of Ni. When Fe(III) was present at more than 5× the mass of Ni, competition occurs for ligand coordination with DMG.[54] For example, if 50 μg Fe(III) were added in the presence of 10 μg Ni, the resulting color band for Ni would travel ~20 ± 2 mm (*vs.* ~7 mm for 10 μg Ni alone). This was likely a consequence of the higher solubility of the $Fe(DMG)_2(OH)_2$ complex, based on infrared absorbance spectra data, than the $Ni(DMG)H_2$ complex.[54] Of interest however, was that the distance traveled by the color band was predictable, suggesting that a correction factor could be implemented to account for the presence of Fe(III).

Table 2 Matrix interferences evaluated by tolerance ratios. Analytes, Fe, Ni, and Cu, were held at 10 μg and the mass of each interfering metal species was varied according to the ratio (μg interference per μg analyte)

	10% tolerance ratio		
Interfering ion	Ni	Cu	Fe
Ni(II)	—	≥10	0.5
Fe(II)	≥10	≥10	—
Fe(III)	5	≥10	≥10
Cu(II)	1	—	≥10
Zn(II)	≥10	≥10	1
Co(III)	1	≥10	1
Cd(II)	≥10	≥10	≥10
Pb(II)	≥10	≥10	≥10
Mn(II)	≥10	≥10	≥10
V(III)	1	≥10	1
Cr(VI)	10	5	0.5
Mg(II)	≥10	≥10	≥10
Al(III)	1	≥10	5
Ba(II)	≥10	≥ 10	≥ 10

3.6 Welding fume reference material

A certified stainless steel reference fume was digested and assayed for Fe, Ni, and Cu with the multi-channel device. Results are presented in Table 3. Three different fume samples were tested, each in triplicate. In the first sample, trace levels of Cu were below the detection limit of the device. Standard addition of 5 μg Cu was used for two other samples. Percent recovery was close to 100%. The percent error for detection of low (<10 μg) metal mass was due to high relative percent error, but this was because distance was measured visually to the nearest half mm, which was a non-insignificant percent of the measured color band distance. For example, 5 μg Cu is expected to form a color band approximately 8-mm long, but a variance of only 1 mm is a significant fraction (12.5%) of the nominal distance of the band. This represents a limitation of our system when measuring analyte mass near the detection limit. Reference samples used for testing were in powder form, but typically, welding fumes would be collected through collection of the fume onto air sampling filters. Metals would be subject to acid digestion procedures, as described previously.[10] Although additional sample preparation would be necessary in this event, digestion would be carried out with small filters (1–10 mm diameter), which would require small (μL) reagent volumes and some power (*e.g.* low-wattage microwave), both which represent improvements over traditional preparation methods.

Conclusions

Paper microfluidics presents many advantages over traditional analytical instruments for exposure monitoring, such

Table 3 Ni, Cu, and Fe detection from certified welding fumes. Reference fume was certified for Fe, Mn, and Zn. n = 3

	Actual level (μg)			Measured level (μg)			Percent recovery (%)		
WF sample	Fe	Ni	Cu	Fe	Ni	Cu	Fe	Ni	Cu
119_11	59.6	7.4	Trace	57 ± 4.5	6.9 ± 1.6	—	96 ± 7.6	93 ± 21	—
119_21	59.6	7.4	5.0	65 ± 4.7	7.5 ± 0.9	4.5 ± 2.0	109 ± 7.9	102 ± 12	90 ± 40
119_31	15.0	6.9	5.0	15 ± 2.1	9.0 ± 4.5	5.1 ± 1.5	99 ± 14	131 ± 66	102 ± 30

as portability, cost, ease-of-use, and complexity of operation. Colorimetric detection is one of the most commonly utilized detection motifs in paper microfluidics; however, the need for external detection tools makes the technique less ideal for on-site application. Distance-based detection captures the simplicity of colorimetric measurement but is more cost effective for widespread deployment. In this work, we utilized the precision and gradient-printing capabilities of commercial inkjet printing to extend the dynamic range of distance-based detection for Ni and Cu, and improve the linearity for Fe. As was demonstrated, the multi-channel device can measure Ni, Cu, and Fe simultaneously from many sources of metal particulates (*e.g.* welding fumes) with minimal matrix effects on the analytical signal.

Acknowledgements

We would like to thank Dr. Owen Butler for developing the HSL stainless and mild steel welding reference fumes used in this project. This work was supported by grants from the State of Colorado, Colorado State University, the National Science Foundation (1415655) and the National Institute of Occupational Safety and Health (R21OH010050).

References

1 C. A. Pope III, M. J. Thun, M. M. Namboodiri, D. W. Dockery, J. S. Evans, F. E. Speizer and C. W. Heath Jr, *Am. J. Respir. Cell Mol. Biol.*, 1995, **151**, 669–674.
2 United States Environmental Protection Agency, Nickel Compounds, http://www.epa.gov/ttnatw01/hlthef/nickel.html, (accessed March 2015).
3 W. M. Draper, K. Ashley, C. R. Glowacki and P. R. Michael, *Anal. Chem.*, 1999, **71**, 33–60.
4 M. R. Gomez, S. Cerutti, L. L. Sombra, M. F. Silva and L. D. Martínez, *Food Chem. Toxicol.*, 2007, **45**, 1060–1064.
5 J.-P. Goullé, L. Mahieu, J. Castermant, N. Neveu, L. Bonneau, G. Lainé, D. Bouige and C. Lacroix, *Forensic Sci. Int.*, 2005, **153**, 39–44.
6 C. C. Conrad and K. G. Hilchey, *Environ. Monit. Assess.*, 2011, **176**, 273–291.
7 M. M. Mentele, J. Cunningham, K. Koehler, J. Volckens and C. S. Henry, *Anal. Chem.*, 2012, **84**, 4474–4480.
8 S. Z. Hossain and J. D. Brennan, *Anal. Chem.*, 2011, **83**, 8772–8778.
9 A. Apilux, W. Dungchai, W. Siangproh, N. Praphairaksit, C. S. Henry and O. Chailapakul, *Anal. Chem.*, 2010, **82**, 1727–1732.
10 D. M. Cate, P. Nanthasurasak, P. Riwkulkajorn, C. L'Orange, C. S. Henry and J. Volckens, *Ann. Occup. Hyg.*, 2014, met078.
11 G. G. Lewis, J. S. Robbins and S. T. Phillips, *Chem. Commun.*, 2014, **50**, 5352–5354.
12 S. Z. Hossain, R. E. Luckham, M. J. McFadden and J. D. Brennan, *Anal. Chem.*, 2009, **81**, 9055–9064.
13 B. M. Jayawardane, S. Wei, I. D. McKelvie and S. D. Kolev, *Anal. Chem.*, 2014, **86**, 7274–7279.
14 R. V. Taudte, A. Beavis, L. Wilson-Wilde, C. Roux, P. Doble and L. Blanes, *Lab Chip*, 2013, **13**, 4164–4172.
15 W. Dungchai, Y. Sameenoi, O. Chailapakul, J. Volckens and C. S. Henry, *Analyst*, 2013, **138**, 6766–6773.
16 Y. Sameenoi, P. Panymeesamer, N. Supalakorn, K. Koehler, O. Chailapakul, C. S. Henry and J. Volckens, *Environ. Sci. Technol.*, 2012, **47**, 932–940.
17 D. M. Cate, J. A. Adkins, J. Mettakoonpitak and C. S. Henry, *Anal. Chem.*, 2014, **87**, 19–41.
18 A. K. Yetisen, M. S. Akram and C. R. Lowe, *Lab Chip*, 2013, **13**, 2210–2251.
19 A. K. Ellerbee, S. T. Phillips, A. C. Siegel, K. A. Mirica, A. W. Martinez, P. Striehl, N. Jain, M. Prentiss and G. M. Whitesides, *Anal. Chem.*, 2009, **81**, 8447–8452.
20 S. C. Lou, C. Patel, S. Ching and J. Gordon, *Clin. Chem.*, 1993, **39**, 619–624.
21 G. G. Lewis, M. J. DiTucci and S. T. Phillips, *Angew. Chem.*, 2012, **124**, 12879–12882.
22 Y. Zhang, C. Zhou, J. Nie, S. Le, Q. Qin, F. Liu, Y. Li and J. Li, *Anal. Chem.*, 2014, **86**, 2005–2012.
23 G. G. Lewis, J. S. Robbins and S. T. Phillips, *Anal. Chem.*, 2013, **85**, 10432–10439.
24 R. Zuk, V. Ginsberg, T. Houts, J. Rabbie, H. Merrick, E. Ullman, M. Fischer, C. Sizto, S. Stiso and D. Litman, *Clin. Chem.*, 1985, **31**, 1144–1150.
25 D. M. Cate, W. Dungchai, J. C. Cunningham, J. Volckens and C. S. Henry, *Lab Chip*, 2013, **13**, 2397–2404.
26 R. Masoodi, *MS Thesis*, The University of Wisconsin-Milwaukee, 2010.
27 R. Masoodi and K. M. Pillai, *AIChE J.*, 2010, **56**, 2257–2267.
28 R. Masoodi, H. Tan and K. M. Pillai, *AIChE J.*, 2012, **58**, 2536–2544.
29 D. J. Cohen, R. C. Morfino and M. M. Maharbiz, *PLoS One*, 2009, **4**, e7086.
30 B. Derby, *J. Mater. Chem.*, 2008, **18**, 5717–5721.
31 N. Komuro, S. Takaki, K. Suzuki and D. Citterio, *Anal. Bioanal. Chem.*, 2013, **405**, 5785–5805.
32 K. Abe, K. Suzuki and D. Citterio, *Anal. Chem.*, 2008, **80**, 6928–6934.
33 X. Li, J. Tian, G. Garnier and W. Shen, *Colloids Surf., B*, 2010, **76**, 564–570.
34 K. Abe, K. Kotera, K. Suzuki and D. Citterio, *Anal. Bioanal. Chem.*, 2010, **398**, 885–893.
35 K. Maejima, S. Tomikawa, K. Suzuki and D. Citterio, *RSC Adv.*, 2013, **3**, 9258–9263.
36 S. Z. Hossain, R. E. Luckham, A. M. Smith, J. M. Lebert, L. M. Davies, R. H. Pelton, C. D. Filipe and J. D. Brennan, *Anal. Chem.*, 2009, **81**, 5474–5483.
37 W. W. Yu and I. M. White, *Anal. Chem.*, 2010, **82**, 9626–9630.
38 W. Y. Wei and I. M. White, *Analyst*, 2013, **138**, 1020–1025.
39 University of Washington, MicroFluidics 2.0, http://www.mf20.org/, (accessed March 2015).
40 E. Tekin, P. J. Smith and U. S. Schubert, *Soft Matter*, 2008, **4**, 703–713.

41 W. D. Jacobs and J. H. Yoe, *Anal. Chim. Acta*, 1959, **20**, 332–339.
42 M. Soylak and N. D. Erdogan, *J. Hazard. Mater.*, 2006, **137**, 1035–1041.
43 K. D. Charleton, A. E. Smith and D. M. Goltz, *Anal. Lett.*, 2009, **42**, 2533–2546.
44 V. Rouchon, M. Duranton, O. Belhadj, M. Bastier-Deroches, V. Duplat, C. Walbert and B. V. Hansen, *Polym. Degrad. Stab.*, 2013, **98**, 1339–1347.
45 F. E. Grubbs, *Ann. Math. Stat.*, 1950, 27–58.
46 A. Paul, *Anal. Chem.*, 1963, **35**, 2119–2121.
47 E. Schlemper and R. K. Murmann, *Inorg. Chem.*, 1983, **22**, 1077–1081.
48 G. F. Smith, W. H. McCurdy and H. Diehl, *Analyst*, 1952, **77**, 418–422.
49 E. W. Washburn, *Phys. Rev.*, 1921, **17**, 273.
50 United States Department of Labor, Occupational exposure to hazardous chemicals in laboratories., https://www.osha.gov/pls/oshaweb/owadisp.show_document?p_id=10106&p_table=STANDARDS, (accessed March 2015).
51 Center for Disease Control and Prevention, NIOSH Pocket Guide to Chemical Hazards, http://www.cdc.gov/niosh/npg/pgintrod.html, (accessed March 2015).
52 J. T. Karlsen, G. Farrants, T. Torgrimsen and A. Reith, *AIHA J.*, 1992, **53**, 290–297.
53 S. Chaiyo, O. Chailapakul, T. Sakai, N. Teshima and W. Siangproh, *Talanta*, 2013, **108**, 1–6.
54 K. Burger, I. Ruff and F. Ruff, *J. Inorg. Nucl. Chem.*, 1965, **27**, 179–190.

